

Human Motion to Humanoid Control



10 December 2021

Sridath TULA and Adithya BALAJI

IMARO, Ecole Centrale de Nantes

Modified Hanavan Model

Abstract

The main objective of this lab is to study how to determine the efforts implied in a human motion by capturing the motion data in order to simulate and analyze how closely we reproduce the particular motion of Actor.

Contents

| | | |
|----------|---|-----------|
| 1 | Introduction | 2 |
| 1.1 | Modified Hanavan Model | 2 |
| 2 | Single Pendulum | 6 |
| 2.1 | Position | 7 |
| 2.2 | Velocity | 7 |
| 2.3 | Acceleration | 7 |
| 2.4 | Forces and Torque | 8 |
| 2.5 | Result | 8 |
| 3 | Double Pendulum | 8 |
| 3.1 | Position | 9 |
| 3.2 | Velocity | 9 |
| 3.3 | Acceleration | 10 |
| 3.4 | Forces and Torque | 10 |
| 3.5 | Result | 10 |
| 4 | Experimentation | 11 |
| 4.1 | Objective | 11 |
| 4.2 | Working Hypotheses | 11 |
| 4.3 | Experimental conditions and Devices | 11 |
| 5 | Simulation Results | 12 |
| 5.1 | Simple arm motion | 12 |
| 5.2 | Kicking Motion with Legs | 14 |
| 5.3 | Jumping Motion | 16 |
| 5.4 | Sitting Motion | 19 |
| 6 | Synthesis | 19 |
| 7 | Conclusion | 20 |
| | Bibliography | 21 |

List of Figures

| | | |
|---|--|---|
| 1 | Modified Hanavan Model Segmentation | 3 |
| 2 | Hanavan Model Parameters | 4 |
| 3 | Hanavan Model Geometry Shapes Segmentation | 4 |
| 4 | Geometric shapes in Hanavan Model | 5 |
| 5 | Geometric shapes in Hanavan Model | 6 |
| 6 | Geometric shapes in Hanavan Model | 6 |
| 7 | Single Inverted Pendulum | 7 |

| | | |
|----|------------------------------------|----|
| 8 | Inverted Single Pendulum | 8 |
| 9 | Double Pendulum | 9 |
| 10 | Inverted Double Pendulum | 10 |

1 Introduction

The purpose of this lab is to study how to determine the efforts implied in a human motion from a set of given kinematics data. This data of the motion of a human body come from a camera motion capture. In this study, make use of Modified Hanavan model which is a method widely used in Biomechanics and Anatomy in the study of the human body to estimate the mass of the different segments of the human body. The parameters obtained from measuring our actor are to be used to calculate the Dynamics of the model using the Newton-Euler method to obtain the forces, velocity, and accelerations of the body in motionFirst, simple examples of the computation of torques with the Newton-Euler method will be detailed for the case of the single pendulum and double pendulum models. Then, it will be presented how to modelize a human body through the modified Hanavan model and how to apply this model to a specific subject. Afterwards, The dynamics calculated are then used to rebuild the motion of this body in a simulation to see how natural the captured motion is, we also make use of a force sensor to make comparison of the forces acting on the body.

1.1 Modified Hanavan Model

The Modified Hanavan model(figure[1]) was first proposed in 1964 and then modified in 1975. This model proposed to subdivide the human body into segments. The trunk was divided into 3 segments, with each a cylinder, the hand was chosen to be an ellipsoid of revolution and the foot was defined to be an elliptical solid with circular proximal ends. The Thigh was also defined to be an elliptical solid with circular distal ends.

The Modified Hanavan model requires 41 parameters to be measured in the body of the actor. the figure[2] shows the parameters required to measure using Measuring tape.

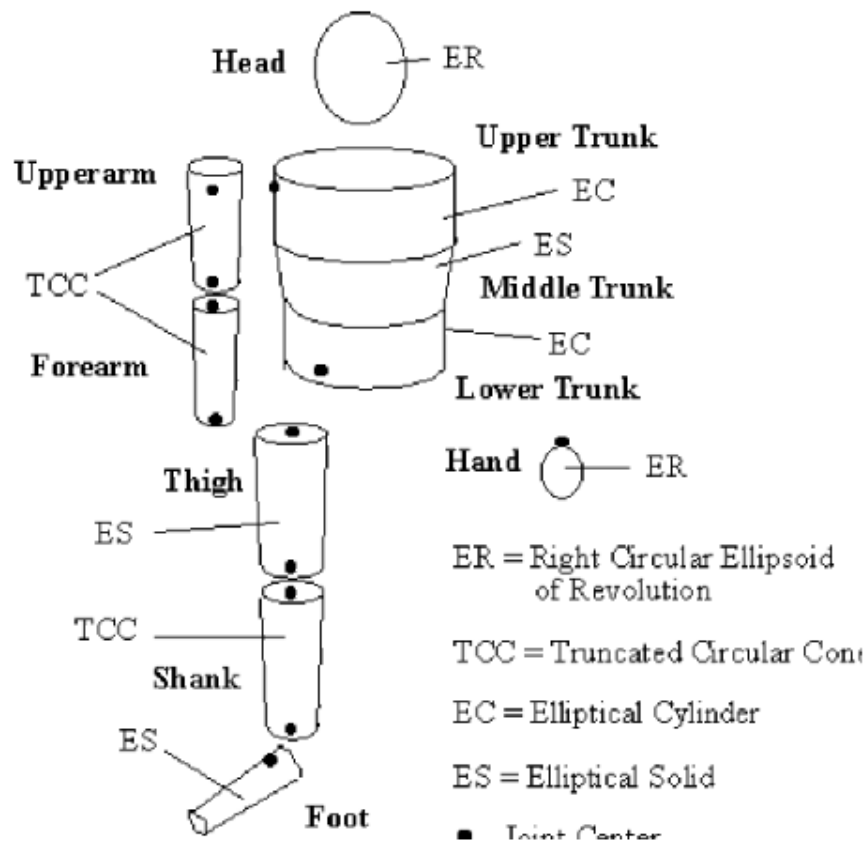


Figure 1: Modified Hanavan Model Segmentation

Therefore, to apply the modified Hanavan biomechanical model to a human body, one must determine adapted dimension of each modelized body to the subject. For that, one has to determine the Hanavan parameters presented in the Figure 8 by measuring some length, circumference, width and depth. A tape measure can be used to perform the measurements. Once these parameters are found, the geometrical parameter of each body can be found using the formulas

| No | Parameter | No | Parameter |
|----|--|----|--|
| 1 | L: Hand | 21 | C: Toe |
| 2 | L: Wrist to Knuckle | 22 | C: Ankle |
| 3 | L: Forearm | 23 | C: Shank |
| 4 | L: Upper arm | 24 | C: Knee |
| 5 | L: Elbow to Acromion | 25 | C: Upper Thigh |
| 6 | L: Foot | 26 | C: Head |
| 7 | L: Shank | 27 | C: Chest |
| 8 | L: Thigh | 28 | C: Xyphion Level |
| 9 | L: Head | 29 | C: Omphalion Level |
| 10 | L: Upper Trunk | 30 | C: Buttock |
| 11 | L: Xyphion to Acromion Level | 31 | W: Hand |
| 12 | L: Middle Trunk | 32 | W: Wrist |
| 13 | L: Lower Trunk | 33 | W: Foot |
| 14 | C: Fist | 34 | W: Toe |
| 15 | C: Wrist | 35 | D: Hip |
| 16 | C: Forearm | 36 | W: Chest |
| 17 | C: Elbow | 37 | W: Xyphion Level |
| 18 | C: Axillary Arm | 38 | W: Omphalion Level |
| 19 | C: Foot | 39 | W: Coxae |
| 20 | C: Ball of Foot | 40 | L: Xyphion Level to Chin/Neck Intersection |
| 41 | L: Hip to Chin/Neck Intersection = P12 + P13 + P40 | | |

L: Length; C: Circumference; W: Width; D: Depth

Figure 2: Hanavan Model Parameters

After we measure the 41 parameters as mentioned in figure[2], we use them as arguments to BSP functions which help us to estimate the parameters of the geometric shapes that these human body segments have been approximated to. These functions are shown below in figure[3]

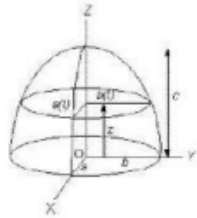
| Segment | Shape | Group | Arguments |
|----------|---------------|-------|--|
| Hand | ER | SE | $a = b = \frac{P_{14}}{2\pi}, c = \frac{P_2}{2}$ |
| Forearm | TCC | ES | $a_0 = b_0 = \frac{P_{17}}{2\pi}, a_1 = b_1 = \frac{P_{15}}{2\pi}, L = P_3$ |
| Upperarm | TCC | ES | $a_0 = b_0 = \frac{P_{18}}{2\pi}, a_1 = b_1 = \frac{P_{17}}{2\pi}, L = P_5$ |
| Foot | ES Circ. Base | ES | $a_0 = b_0 = \frac{P_{19}}{2\pi}, a_1 = \frac{P_{33}+P_{34}}{4}, b_1 = \frac{P_{20}+P_{21}}{2\pi}, L = P_6$ |
| Shank | TCC | ES | $a_0 = b_0 = \frac{P_{24}}{2\pi}, a_1 = b_1 = \frac{P_{22}}{2\pi}, L = P_7$ |
| Thigh | ES Circ. Top | ES | $b_0 = \frac{P_{35}}{2}, a_0 = \frac{P_{25}}{\pi} - b_0, a_1 = b_1 = \frac{P_{24}}{2\pi}, L = P_8$ |
| Head | ER | SE | $a = b = \frac{P_{26}}{2\pi}, c = \frac{P_9}{2}$ |
| U Trunk | EC | ES | $a_0 = a_1 = \frac{P_{36}+P_{37}}{4}, b_0 = b_1 = \frac{P_{27}+P_{28}}{2\pi} - a_0, L = P_{11}$ |
| M Trunk | ES | ES | $a_0 = \frac{P_{37}}{2}, a_1 = \frac{P_{38}}{2}, L = P_{12}, b_0 = \frac{P_{28}}{\pi} - a_0, b_1 = \frac{P_{29}}{\pi} - a_1$ |
| L Trunk | EC | ES | $a_0 = a_1 = \frac{P_{38}+P_{39}}{4}, L = P_{13}, b_0 = b_1 = \frac{P_{29}+P_{30}}{2\pi} - a_0$ |

EC: Elliptical Column, ER: Ellipsoid of Revolution, ES: Elliptical Solid, SE:

Semi-Ellipsoid, TCC Truncated Circular Cone

Figure 3: Hanavan Model Geometry Shapes Segmentation

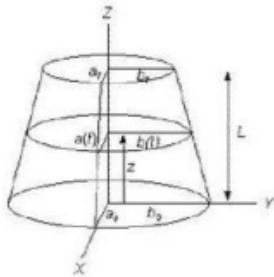
Thus the segments that are approximated to a geometric shape has five Parameters which are required to calculate its dynamics when it is in motion. These BSP parameters are Mass, Position of centre of Mass, moment of Inertia Ixx,Iyy,Izz. the formulation is shown in the figure[4].



| | |
|----------|--|
| Mass | $\frac{2\pi}{3} \rho abc$ |
| CoM pos | $\frac{3}{8}c$ |
| I_{xx} | $\frac{1}{5}m[(b^2 + c^2) - (\frac{3}{8}c)^2]$ |
| I_{yy} | $\frac{1}{5}m[(a^2 + c^2) - (\frac{3}{8}c)^2]$ |
| I_{zz} | $\frac{1}{5}m(a^2 + b^2)$ |

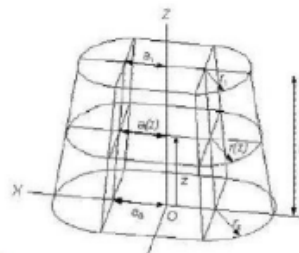
(a) Semi-Ellipsoid group

Elliptical solid (ES)



| | |
|----------|--|
| Mass | $\pi \rho L A_1^{ab}$ |
| CoM pos | $L \frac{A_2^{ab}}{A_1^{ab}}$ |
| I_{xx} | $\frac{1}{4}m \frac{A_3^{abbb}}{A_1^{ab}} + mL^2 \frac{A_3^{ab}}{A_1^{ab}} - m(L \frac{A_2^{ab}}{A_1^{ab}})^2$ |
| I_{yy} | $\frac{1}{4}m \frac{A_4^{aabb}}{A_1^{ab}} + mL^2 \frac{A_3^{ab}}{A_1^{ab}} - m(L \frac{A_2^{ab}}{A_1^{ab}})^2$ |
| I_{zz} | $\frac{1}{4}m \frac{A_3^{aab} + A_4^{abbb}}{A_1^{ab}}$ |

(b) Elliptical Solid group



Stadium solid (SS)

| | |
|----------|--|
| Mass | $\rho L(4A_1^{ar} + \pi A_1^{rr})$ |
| CoM | $L \frac{4A_1^{ar} + \pi A_1^{rr}}{4A_1^{ar} + \pi A_1^{rr}}$ |
| I_{xx} | $\frac{m}{4A_1^{ar} + \pi A_1^{rr}} \left(\frac{4L}{3} A_4^{arrr} + \frac{\pi L}{4} A_4^{rrrr} + 4L^3 A_3^{ar} + \frac{\pi L^3}{2} A_3^{rr} - \frac{(4A_3^{ar} + \pi A_3^{rr})^2}{4A_1^{ar} + \pi A_1^{rr}} \right)$ |
| I_{yy} | $\frac{m}{4A_1^{ar} + \pi A_1^{rr}} \left(\frac{4L}{3} A_4^{aarr} + \pi L A_4^{2arr} + \frac{8L}{3} A_4^{arrr} + \frac{\pi L}{4} A_4^{rrrr} + 4L^3 A_3^{ar} + \frac{\pi L^3}{2} A_3^{rr} - \frac{(4A_3^{ar} + \pi A_3^{rr})^2}{4A_1^{ar} + \pi A_1^{rr}} \right)$ |
| I_{zz} | $\frac{mL}{4A_1^{ar} + \pi A_1^{rr}} \left(\frac{4}{3} A_4^{2aar} + \pi A_4^{aarr} + 4A_4^{2arr} + \frac{\pi}{2} A_4^{rrrr} \right)$ |

(c) State Solid group

Figure 4: Geometric shapes in Hanavan Model

| | | | | | | | | | |
|--|------------------------------------|------|------|------|------|------|------|-------------|--------------|
| 1: L: Hand | 19.5 | 18.8 | 18.6 | 20.1 | 18.5 | 18.5 | 18.5 | 18.92857143 | 0.657367069 |
| 2: L: Wrist to Knuckle | 11 | 10 | 10.4 | 11.9 | 11 | 11.3 | 11 | 10.94285714 | 0.6683312552 |
| 3: L: Forearm | 24 | 25 | 26 | 26.9 | 25 | 26 | 27.5 | 25.77442857 | 1.020620726 |
| 4: L: Upper arm | 28 | 32.8 | 28 | 30.5 | 26 | 28 | 32.5 | 29.4 | 2.39200557 |
| 5: L: Elbow to Acromion | 31 | 35.3 | 32.5 | 35.5 | 36 | 32 | 36.5 | 33.88333333 | 2.17342462 |
| 6: L: Foot | 25.2 | 25.2 | 26.6 | 25.5 | 25.6 | 23.5 | 25.5 | 25.47142857 | 0.6524318302 |
| 7: L: Shank | 39.5 | 37.5 | 39.8 | 36.9 | 34 | 35 | 36 | 38.21666667 | 2.052857143 |
| 8: L: Thigh | 35 | 37.2 | 35 | 37.1 | 35 | 38 | 36 | 36.04285714 | 1.10705452 |
| 9: L: Insole | 22.5 | 22.2 | 23.4 | 21.6 | 24 | 23.4 | 22.5 | 22.03333333 | 0.0903317072 |
| 10: L: Upper Trunk | 36 | 21 | 19 | 24.1 | 26 | 19 | 22.5 | 23.8 | 6.3876182321 |
| 11: L: Xyphion to Acromion Level | 21.5 | 21 | 22 | 24.9 | 24 | 22 | 25 | 22.91428571 | 1.531083372 |
| 12: L: Middle Trunk | 10 | 16.2 | 19 | 15.2 | 16 | 19 | 18 | 16.2 | 3.3051475 |
| 13: L: Lower Trunk | 20 | 20.3 | 16 | 18.9 | 23 | 16 | 14 | 18.31428571 | 2.078997354 |
| 14: C: Fist | 23,88333333 | 24 | 26.2 | 25.6 | 26 | 26 | 26.5 | 24.57614285 | 1.069520343 |
| 15: C: Wrist | 16 | 15.8 | 16 | 15.9 | 16 | 16.2 | 17 | 16.12857143 | 0.193916036 |
| 16: C: Forearm | 24,75 | 24.2 | 25.8 | 25.6 | 24 | 26 | 24.5 | 24.97587143 | 0.658147229 |
| 17: C: Elbow | 25 | 23.4 | 24.2 | 24.6 | 25 | 25.5 | 24.5 | 24.67414285 | 0.707253597 |
| 18: C: Lower Arm | 26 | 35.8 | 30.5 | 30.9 | 31 | 36.5 | 33.5 | 33.88333333 | 1.096253597 |
| 19: C: Foot | 24.5 | 27.7 | 24.8 | 23.9 | 23 | 24.8 | 23.5 | 23.88571429 | 0.9181501345 |
| 20: C: Ball of Foot | 23 | 21.6 | 21.5 | 22.3 | 21 | 25 | 19.5 | 21.98571429 | 1.518059312 |
| 21: C: Toe | 22 | 23.3 | 21.8 | 20.7 | 21 | 21.8 | 17.5 | 21.01428571 | 0.616414003 |
| 22: C: Ankle | 25.5 | 26.9 | 23.7 | 23.8 | 24 | 24 | 25.6 | 24.78571428 | 1.284912448 |
| 23: C: Shank | 33.5 | 36.4 | 36 | 35.2 | 36 | 35.8 | 36 | 35.55714286 | 1.0476958837 |
| 24: C: Knee | 36 | 38 | 36.8 | 38.7 | 36 | 37.1 | 37.5 | 37.15714286 | 1.084435337 |
| 25: C: Upper Thigh | 52 | 50.5 | 54.8 | 53.6 | 52 | 53.6 | 52.5 | 52.71428571 | 1.385030759 |
| 26: C: Head | 55.5 | 56.6 | 54.2 | 55.4 | 57 | 57 | 56.5 | 56.02857143 | 1.113103769 |
| 27: C: Chest | 86.5 | 89 | 86.2 | 85 | 85.5 | 86.5 | 86.5 | 86.67414285 | 1.500000000 |
| 28: C: Xyphion Level | 79 | 80 | 79.3 | 77.2 | 78 | 79.7 | 80.2 | 79.77442857 | 0.9579371228 |
| 29: C: Omphalition Level | 73 | 74 | 74.2 | 74 | 73 | 71.5 | 75.5 | 73.6 | 1.206207376 |
| 30: C: Buttock | 93 | 85 | 91 | 94.1 | 97 | 91.8 | 99.5 | 93.05714286 | 4.011196274 |
| 31: W: Hand | 11 | 10.8 | 11 | 10.6 | 10.8 | 11 | 10.5 | 10.81428571 | 0.1632399162 |
| 32: W: Wrist | 6 | 5.9 | 5.5 | 5.7 | 6 | 6.6 | 6.5 | 6.028571429 | 0.3728370736 |
| 33: W: Foot | 9.5 | 9 | 9.3 | 9.6 | 9 | 9.3 | 10.5 | 9.457142857 | 0.2483277404 |
| 34: W: Toe | 9.5 | 9.5 | 10 | 9.5 | 9 | 9.6 | 9.5 | 9.514285714 | 0.3188521743 |
| 35: D: Hip | 15 | 15.5 | 15 | 17.2 | 17 | 15.5 | 17.5 | 16.52857143 | 1.438610434 |
| 36: D: Chest | 30.5 | 28.5 | 29 | 32.2 | 32 | 29 | 30 | 30.17428571 | 1.681428506 |
| 37: D: Xyphion Level | 29.5 | 28 | 27 | 26.4 | 26 | 27 | 28.5 | 27.48871429 | 1.2565697 |
| 38: D: Omphalition Level | 27.5 | 29 | 28 | 29.5 | 26 | 27 | 25 | 27.42857143 | 1.280994449 |
| 39: D: Coxae | 31.5 | 35.5 | 29.5 | 30.4 | 30 | 30 | 34 | 33.55714286 | 2.234946964 |
| 40: L: Xyphion Level to Chin/Neck Intersection | 39 | 31 | 33 | 33.9 | 34 | 33 | 31 | 33.55714286 | 2.6835912 |
| L: Hip to Chin/Neck | 41: Intersection = P12 + P13 + P40 | 69 | 55 | 68 | 68 | 70 | 68 | 66.14285714 | 5.609515725 |

Figure 5: Geometric shapes in Hanavan Model

The above excel sheet shows the 41 measurements taken by different groups for the actor (Robin).

| | Mass(kg) | x | y | z(cm) | Ixx(g*cm^2) | Iyy(g*cm^2) | Izz(g*cm^2) |
|--------------|-------------|---|---|-------------|-------------|-------------|-------------|
| Hand | 0.435171429 | 0 | 0 | 0 | 3666.765975 | 3666.765975 | 2855.32099 |
| Forearm | 4.881485714 | 0 | 0 | 12.88571429 | 278217.8791 | 288992.3413 | 26856.98197 |
| Upper arm | 2.128680952 | 0 | 0 | 16.94166667 | 211863.0678 | 218798.9199 | 23345.88446 |
| Foot | 1.201857143 | 0 | 0 | 13.66450375 | 75962.93088 | 70132.69637 | 14514.62979 |
| Shank | 3.482214286 | 0 | 0 | 19.10833333 | 437365.3068 | 454263.756 | 43992.16922 |
| Thigh | 7.413971429 | 0 | 0 | 17.93160258 | 867377.6893 | 933048.9906 | 195313.3245 |
| Head | 4.606971429 | 0 | 0 | 4.275 | 176171.7489 | 176171.7489 | 146532.808 |
| Upper trunk | 13.77230305 | 0 | 0 | 10.75838457 | 1205838.183 | 1205838.183 | 1217203.487 |
| Middle trunk | 8.996995818 | 0 | 0 | 7.400344933 | 513741.0999 | 557430.0152 | 684851.9209 |
| Lower trunk | 12.14228684 | 0 | 0 | 8.476750545 | 879924.9848 | 879924.9848 | 1090054.033 |

Figure 6: Geometric shapes in Hanavan Model

From the above excel sheet figure we can see that the BSP parameter are measured for the actor.

2 Single Pendulum

A Single inverted pendulum is considered. a point mass m attached to a rotational joint by a mass-less rod.

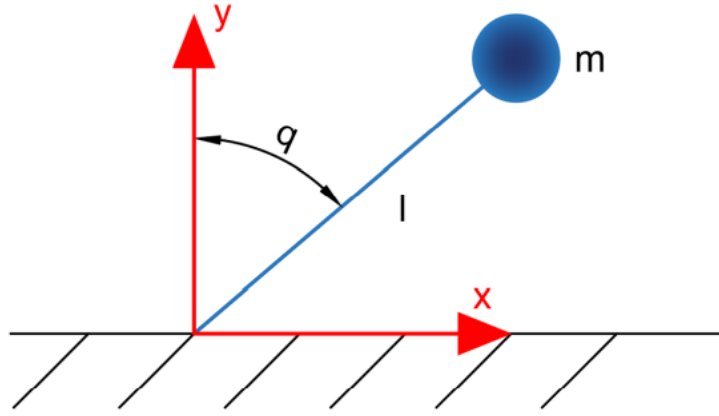


Figure 7: Single Inverted Pendulum

Where m is the mass of the pendulum, l is the length of the link, and q is the angle between the link and the y global axis.

The Mathematical representation of a Single inverted pendulum is derived below :

2.1 Position

The Position of Single inverted pendulum from the above figure is derived as:

$$x_1 = -l \sin(q) \quad (1)$$

$$y_1 = l \cos(q) \quad (2)$$

2.2 Velocity

The Velocity of Single inverted pendulum from the above figure is derived as:

$$\dot{x}_1 = -l_1 \cos(q_1) \dot{q}_1 \quad (3)$$

$$\dot{y}_1 = -l_1 \sin(q_1) \dot{q}_1 \quad (4)$$

2.3 Acceleration

The Acceleration of Single inverted pendulum from the above figure is derived as:

$$\ddot{x}_1 = l_1 \sin(q_1) \dot{q}_1^2 - l_1 \cos(q_1) \ddot{q}_1 \quad (5)$$

$$\ddot{y}_1 = -l_1 \cos(q_1) \dot{q}_1^2 - l_1 \sin(q_1) \ddot{q}_1 \quad (6)$$

2.4 Forces and Torque

The Forces and Torque of Single inverted pendulum from the above figure is derived as:

$$m_1 \ddot{x}_1 = F_{x1} \quad (7)$$

$$m \ddot{y}_1 = F_{y1} - m_1 g \quad (8)$$

$$\tau_1 = m_1 l_1^2 \ddot{q}_1 + m_1 g l_1 \sin(q_1) \quad (9)$$

2.5 Result

Here, we plot the motion of the single Inverted Pendulum with its velocity, acceleration and the reaction forces.thus, We obtain the plot shown in the figure[6]

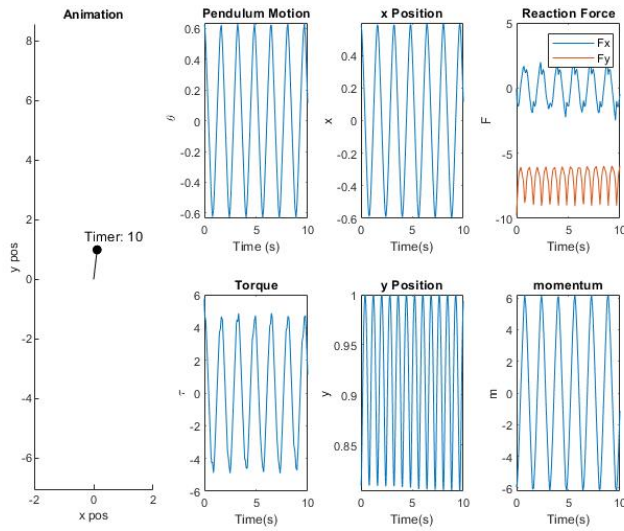


Figure 8: Inverted Single Pendulum

3 Double Pendulum

An inverted double pendulum pendulum is now considered. a point mass m_1 attached to a rotational joint by a mass-less rod and another point mass m_2 attached to the previous point mass by a another mass-less rod.

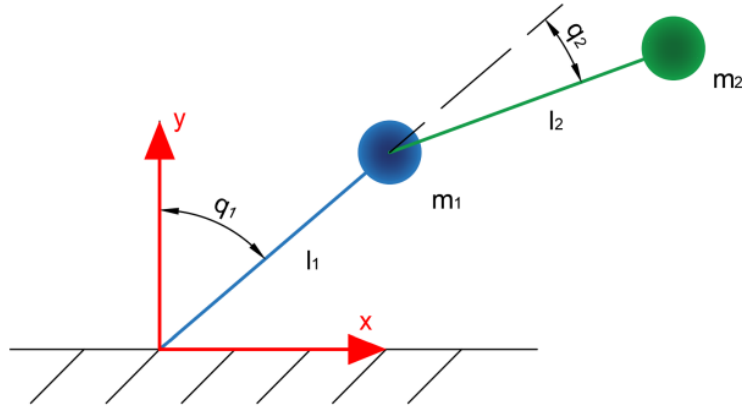


Figure 9: Double Pendulum

Where m_1 and m_2 are the masses of each pendulum, l_1 and l_2 is the length of the link, and q_1 is the angle between the link and the y global axis while q_2 is the angle between link 2 and link 1.

The Mathematical representation of a Double pendulum is derived below :

3.1 Position

The Position of Double pendulum from the above figure is derived as:

$$x_1 = -l_1 \sin(q_1) \quad (10)$$

$$y_1 = l_1 \cos(q_1) \quad (11)$$

$$x_2 = -l_1 \sin(q_1) - l_2 \sin(q_1 + q_2) \quad (12)$$

$$y_2 = l_1 \cos(q_1) + l_2 \cos(q_1 + q_2) \quad (13)$$

3.2 Velocity

The Velocity of Double pendulum from the above figure is derived as:

$$\dot{x}_1 = -l_1 \cos(q_1) \dot{q}_1 \quad (14)$$

$$\dot{y}_1 = -l_1 \sin(q_1) \dot{q}_1 \quad (15)$$

$$\dot{x}_2 = -l_1 \cos(q_1) \dot{q}_1 - l_2 \cos(q_1 + q_2) (\dot{q}_1 + \dot{q}_2) \quad (16)$$

$$\dot{y}_2 = -l_1 \sin(q_1) \dot{q}_1 - l_2 \sin(q_1 + q_2) (\dot{q}_1 + \dot{q}_2) \quad (17)$$

3.3 Acceleration

The Acceleration of Double pendulum from the above figure is derived as:

$$\ddot{x}_1 = l_1 \sin(q_1) \dot{q}_1^2 - l_1 \cos(q_1) \ddot{q}_1 \quad (18)$$

$$\ddot{y}_1 = -l_1 \cos(q_1) \dot{q}_1^2 - l_1 \sin(q_1) \ddot{q}_1 \quad (19)$$

$$\ddot{x}_2 = -l_1 \cos(q_1) \ddot{q}_1 + l_1 \sin(q_1) \dot{q}_1^2 - l_2 \cos(q_1 + q_2) (\ddot{q}_1 + \ddot{q}_2) + l_2 \sin(q_1 + q_2) (\dot{q}_1 + \dot{q}_2)^2 \quad (20)$$

$$\ddot{y}_2 = -l_1 \sin(q_1) \ddot{q}_1 + l_1 \sin(q_1) \dot{q}_1^2 - l_2 \sin(q_1 + q_2) (\ddot{q}_1 + \ddot{q}_2) + l_2 \cos(q_1 + q_2) (\dot{q}_1 + \dot{q}_2)^2 \quad (21)$$

3.4 Forces and Torque

The Forces and Torque of Double pendulum from the above figure is derived as:

$$m_1 \ddot{x}_1 = F_{x1} + F_{x2} \quad (22)$$

$$m_1 \ddot{y}_1 = F_{y1} + F_{y2} - m_1 g \quad (23)$$

$$m_2 \ddot{x}_2 = F_{x2} \quad (24)$$

$$m_2 \ddot{y}_2 = F_{y2} - m_2 g \quad (25)$$

$$\tau_1 = m_1 l_1^2 \ddot{q}_1 + m_1 g l_1 \sin(q_1) \quad (26)$$

$$\tau_2 = m_2 l_2^2 (\ddot{q}_1 + \ddot{q}_2) + m_2 g l_2 \sin(q_1 + q_2) \quad (27)$$

3.5 Result

Here, we plot the motion of the Double Inverted Pendulum with its velocity, acceleration and the reaction forces.thus, We obtain the plot shown in the figure[7]

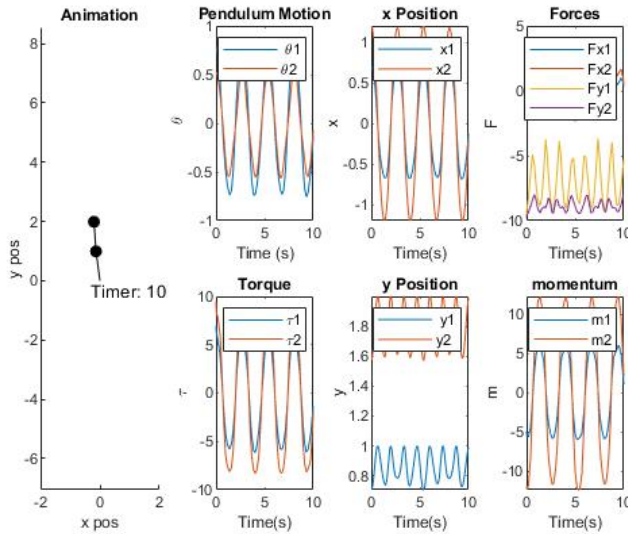


Figure 10: Inverted Double Pendulum

4 Experimentation

4.1 Objective

The objective of this experiment is to capture, simulate and analyze human motion in order to see how closely we can reproduce this motion.

During this experiment, we studied Five kinds of motions that can be easily performed by a human. The motions include: waving, kicking, jumping and sitting on a chair. Each of these motions are performed by an actor(Robin) at different speeds, i.e. slow, medium, fast.

4.2 Working Hypotheses

we have decided to go with three hypotheses.

First,The Hypothesis assumes that the human body segments are rigid and therefore we can apply the Newton-Euler equations. But in reality the outermost body of the human which is the skin on which the motion capture devices are affixed are not rigid and are flexible in nature.

Second, when the moving part is homogeneous.This is particularly important where we use the predictive equations to estimate the mass of the segments by an integration of a point mass over a volume. This property does not correspond to the real human body where the mass distribution is different depending on the segment being considered.

Third, when the Energy Conservative, it means that the sum of the Kinetic Energy and Potential Energy at all times is a constant which means that there is no loss or gain of energy from the environment.

During this experiment, we have studied 5 kinds of motions that could be possibly performed by a human. They include: waving, kicking, jumping and sitting. Each of these motions are performed by an actor at different speeds, i.e. slow, medium, fast.

A population contains a minimum of 10 subjects according to ISB standards, however, we have made this study as a way of learning the methodology and for educational purpose.

4.3 Experimental conditions and Devices

The subject is a Male(Robin). We know that here the study of a single subject cannot be perfect. because as we know that according to ISB standards we should consider 10 minimum subjects. However we studied using single subject for educational purpose.

The measurement of the motion of the actor is done in a closed room equipped with ART track system. This room is cube shaped and contains 8 infra-red cameras which are

positioned on the 4 upper and 4 lower vertices of a cube-shaped room. The subject is equipped with measurement markers in each of his body segments, 15 markers since we are using modified-hanavan method. Each Infra-red cameras is able to detect body markers which have been worn by the actor and calculate the 6 DOF position and orientation. The data collected during this camera measurement is stored in a .drf file for further processing. We use another measurement device which is a force plate to measure the forces from the actor on the ground, this force values are used to compare to the value obtained from the Newton-Euler computation of forces to see how closely we have estimated the measurements.

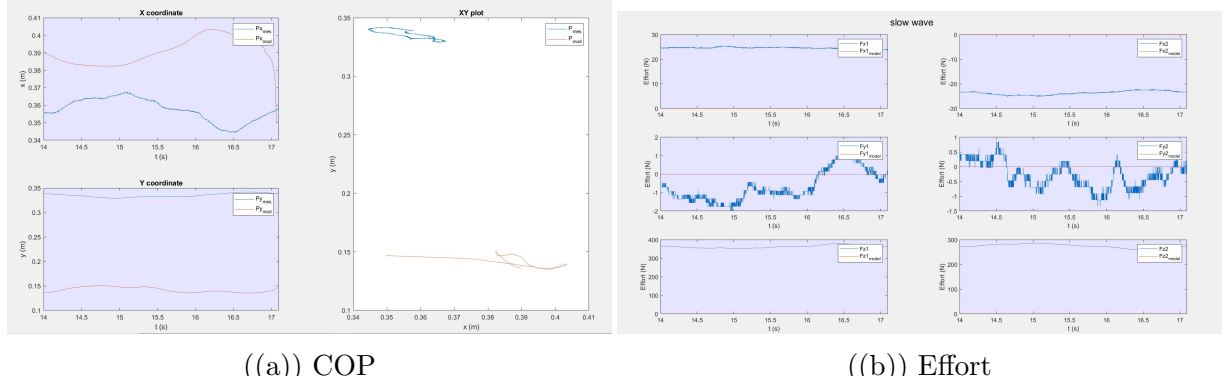
The main thing to follow before opening the ART track system is requires to be calibrated before the use of the system to capture motion. This is important to re-initialize the infrared cameras to ensure that all cameras are able to see all 4 points on a marker. Also if it happens that after calibration, there is a slight push or change in the position of any of the cameras, the entire system needs to be re-calibrated. And also we note that the data capture system is limited by its buffer size, since the camera gives a lot of information per second, therefore it was important for us to only open the system to capture when ready.

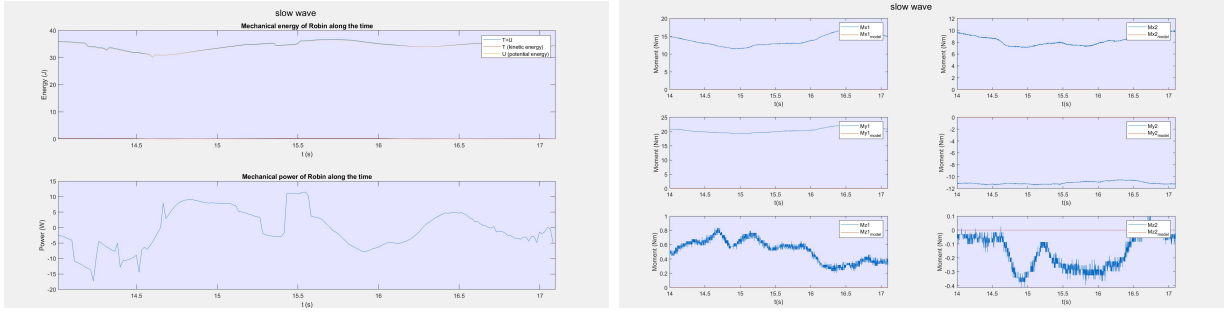
5 Simulation Results

During the Experimentation we asked the actor perform the motions accordingly as shown below.

5.1 Simple arm motion

Here we simulated the results for simple arm motion with different speeds such as slow, Medium and Fast.

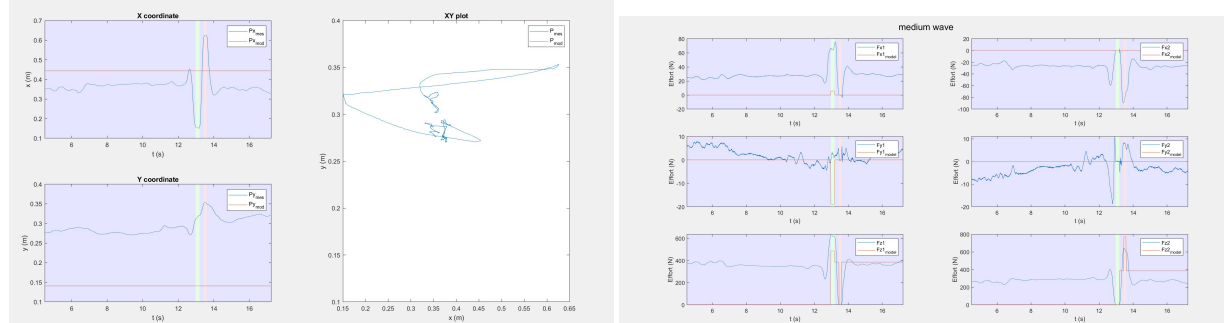




((a)) Energy

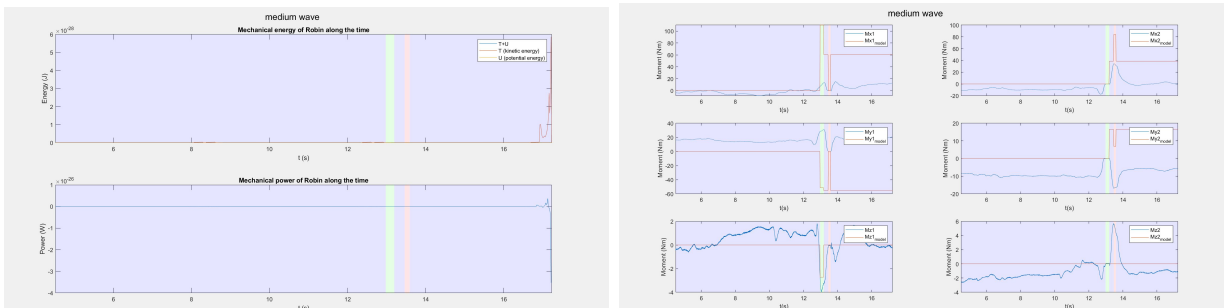
((b)) Moment

The above above plots are for the slow arm motion when the arm moves slowly.



((a)) COP

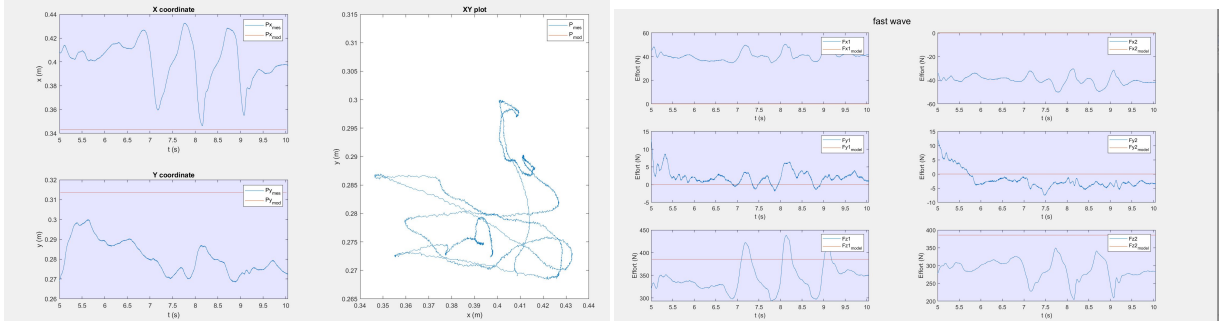
((b)) Effort



((a)) Energy

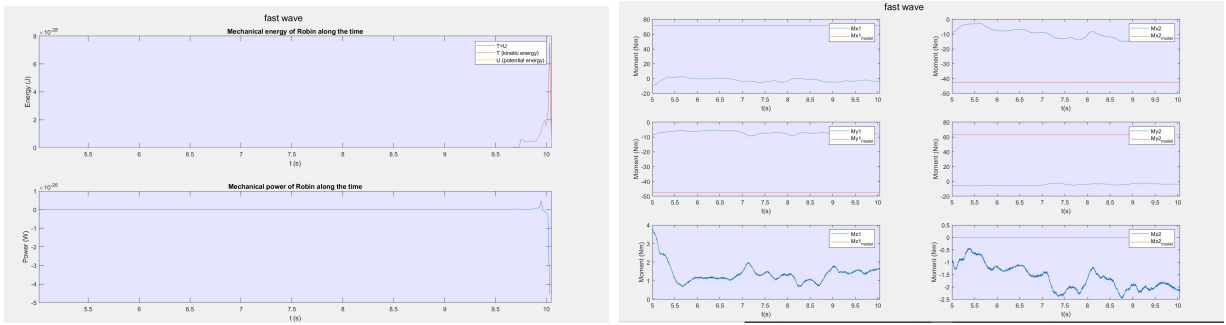
((b)) Moment

The above above plots are for the slow arm motion when the arm moves with medium speed.



((a)) COP

((b)) Effort

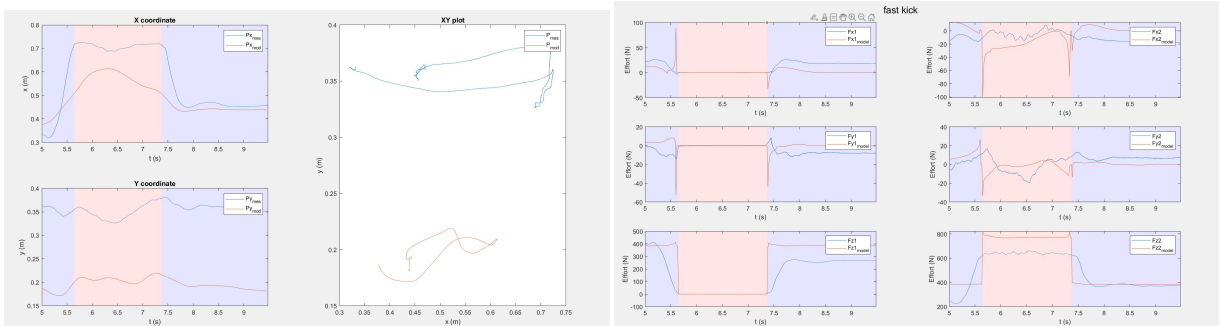


((a)) Energy

((b)) Moment

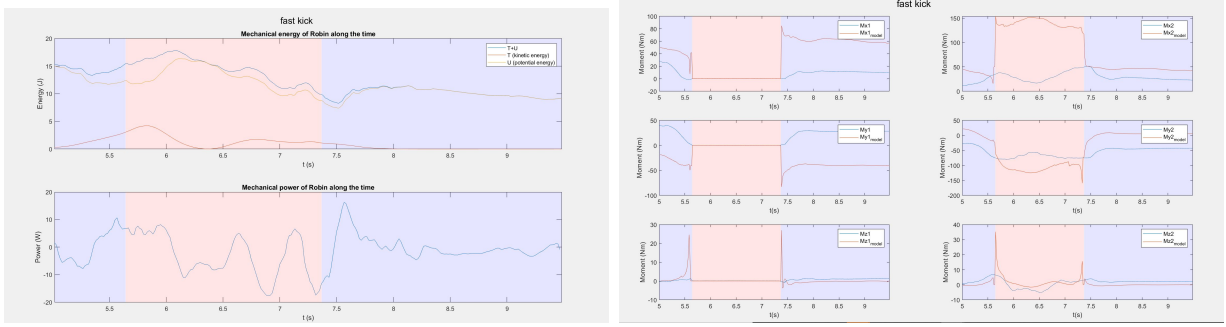
Thus, the above plots represents the simple arm Motion with fast speed.

5.2 Kicking Motion with Legs



((a)) COP

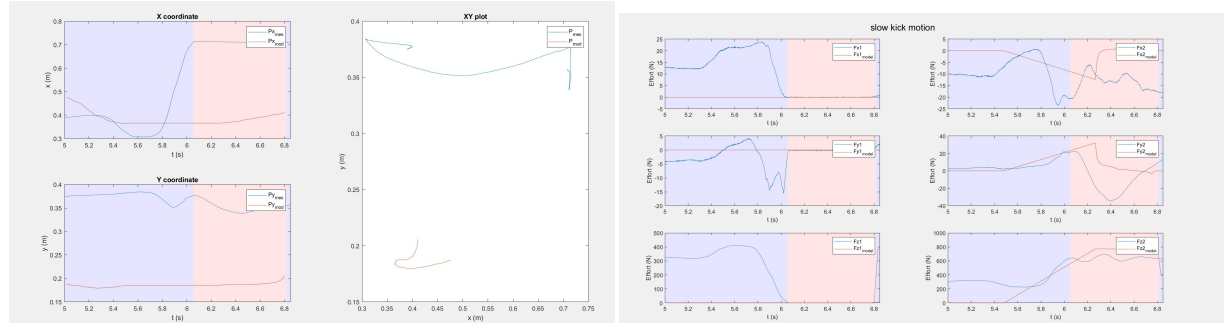
((b)) Effort



((a)) Energy

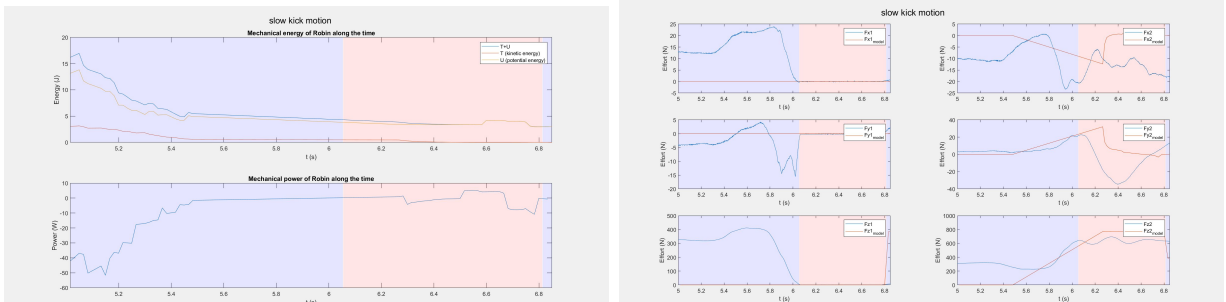
((b)) Moment

The above plots are representation of the leg kick when it is in fast motion.



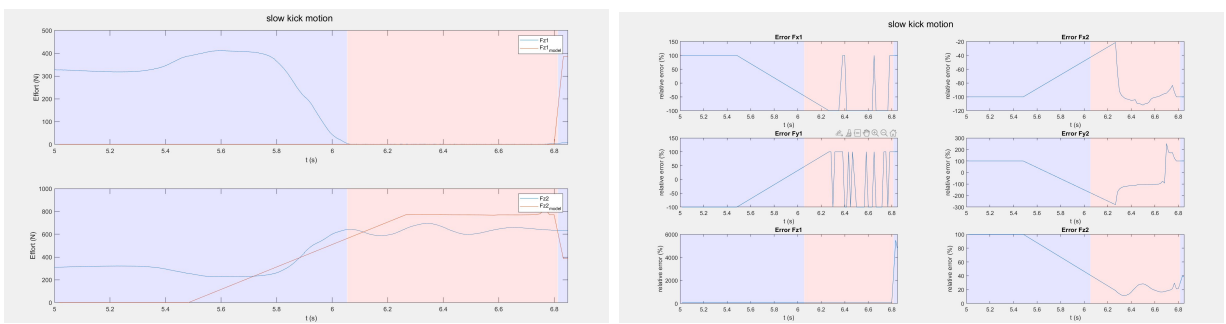
((a)) COP

((b)) Effort



((a)) Energy

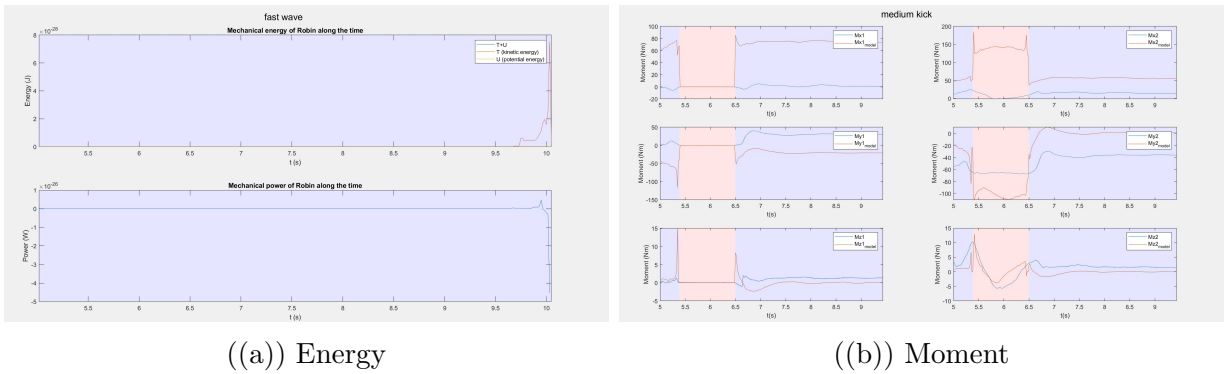
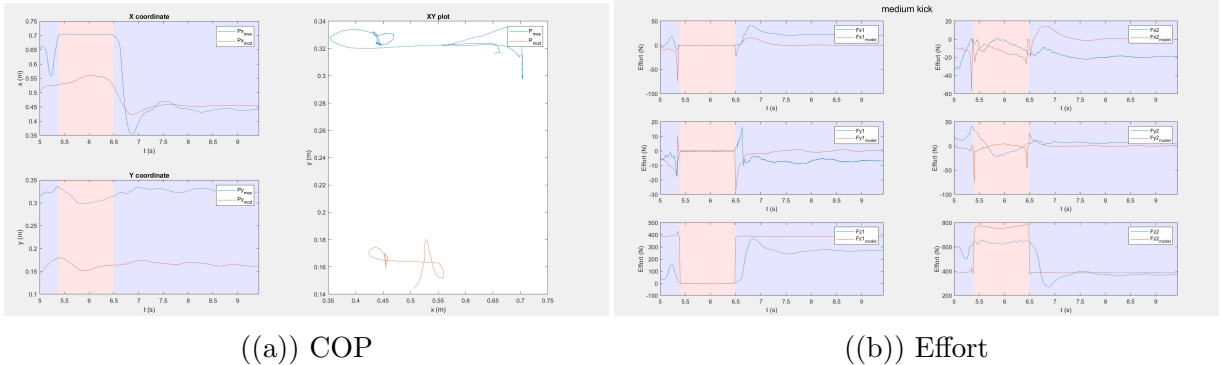
((b)) Moment



((a)) Fz

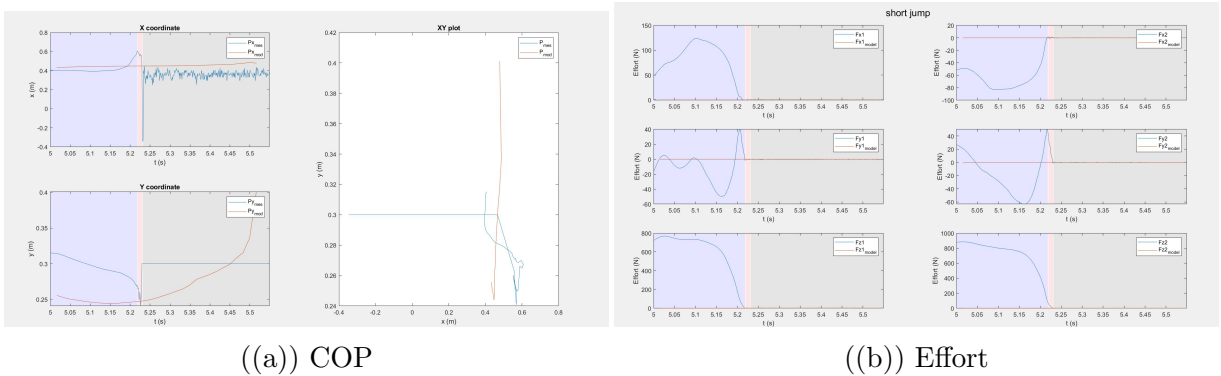
((b)) Effort error

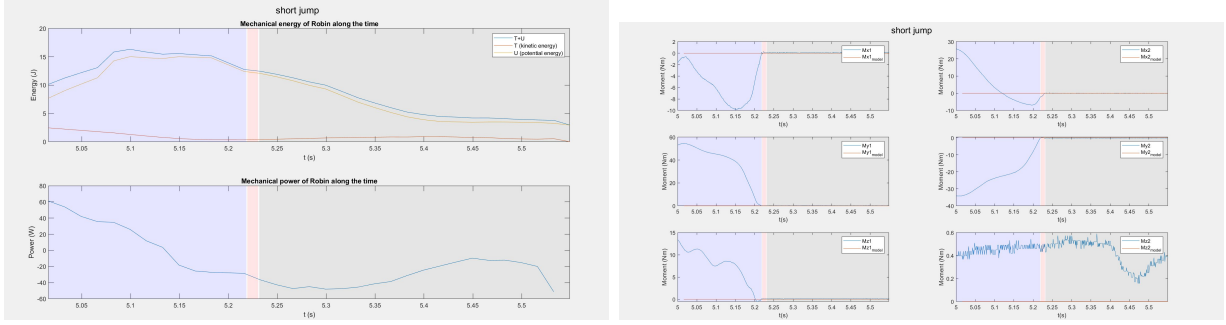
The above plots are representation of the slow kick motion.



The above plots are representation of the leg kick motion with medium speed.

5.3 Jumping Motion

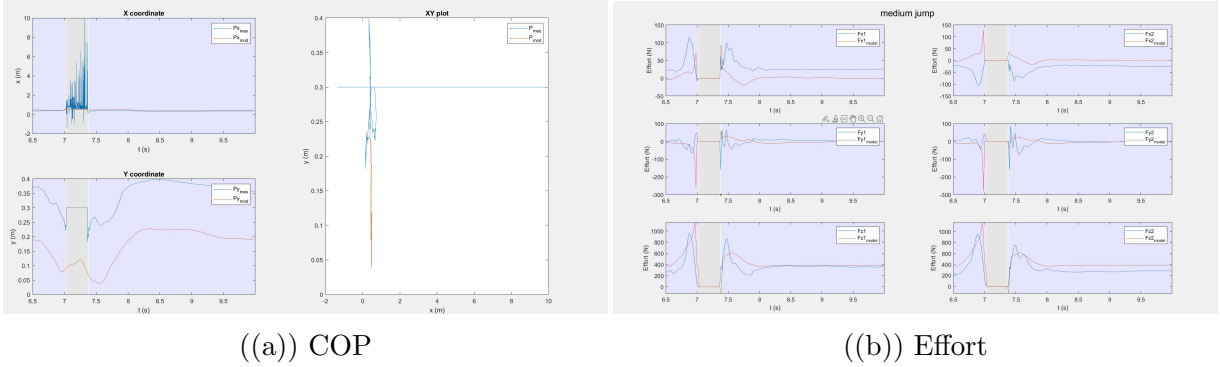




((a)) Energy

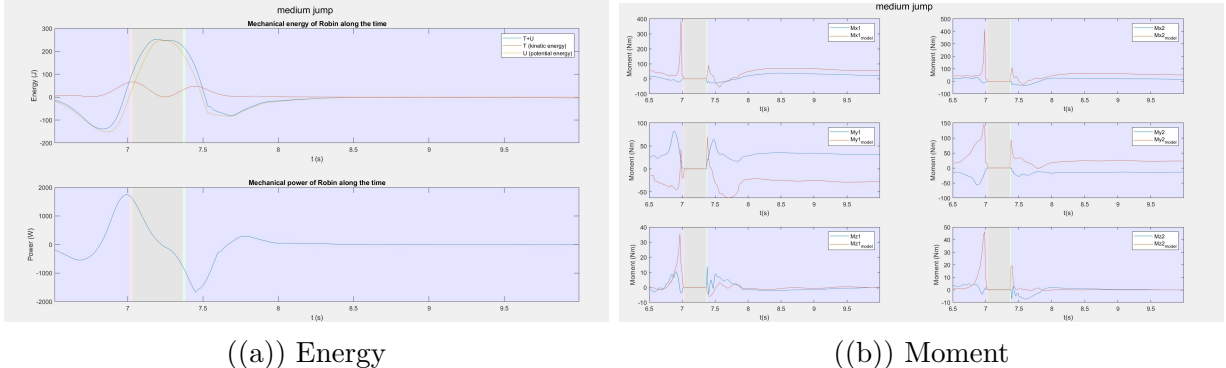
((b)) Moment

The above plots are representation of the short Jump motion.



((a)) COP

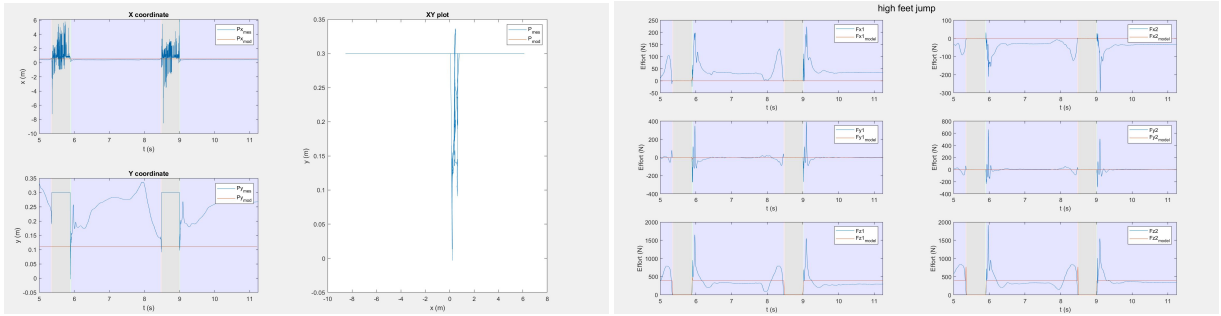
((b)) Effort



((a)) Energy

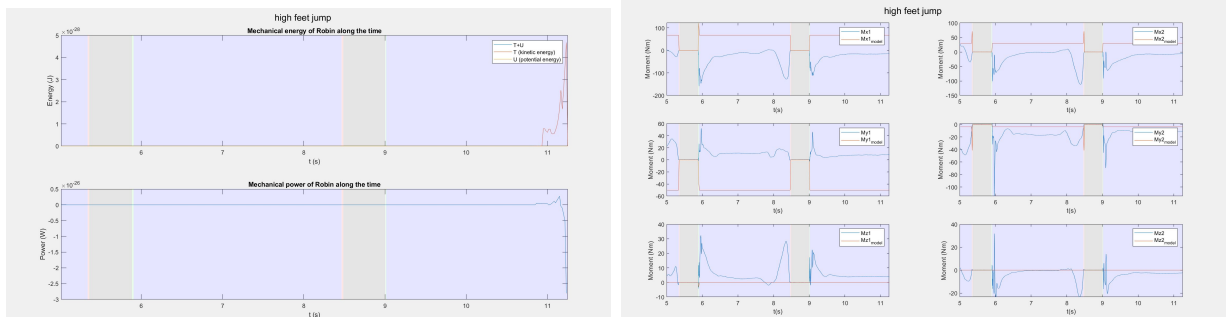
((b)) Moment

The above plots are representation of the Medium Jump motion.



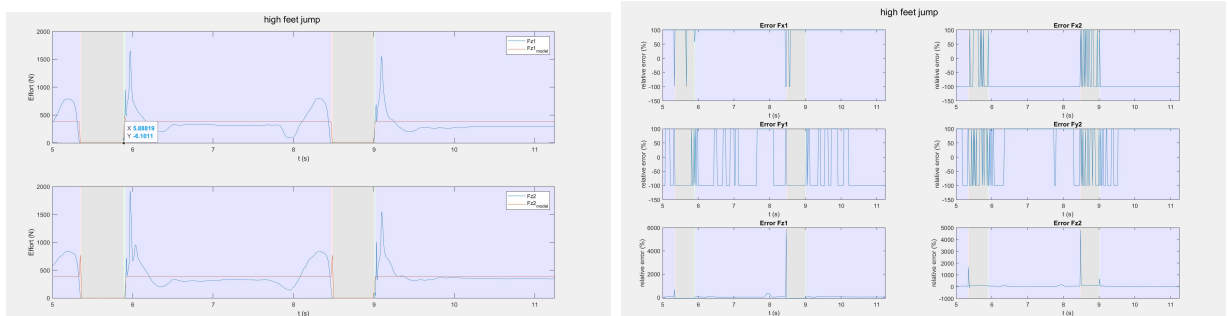
((a)) COP

((b)) Effort



((a)) Energy

((b)) Moment

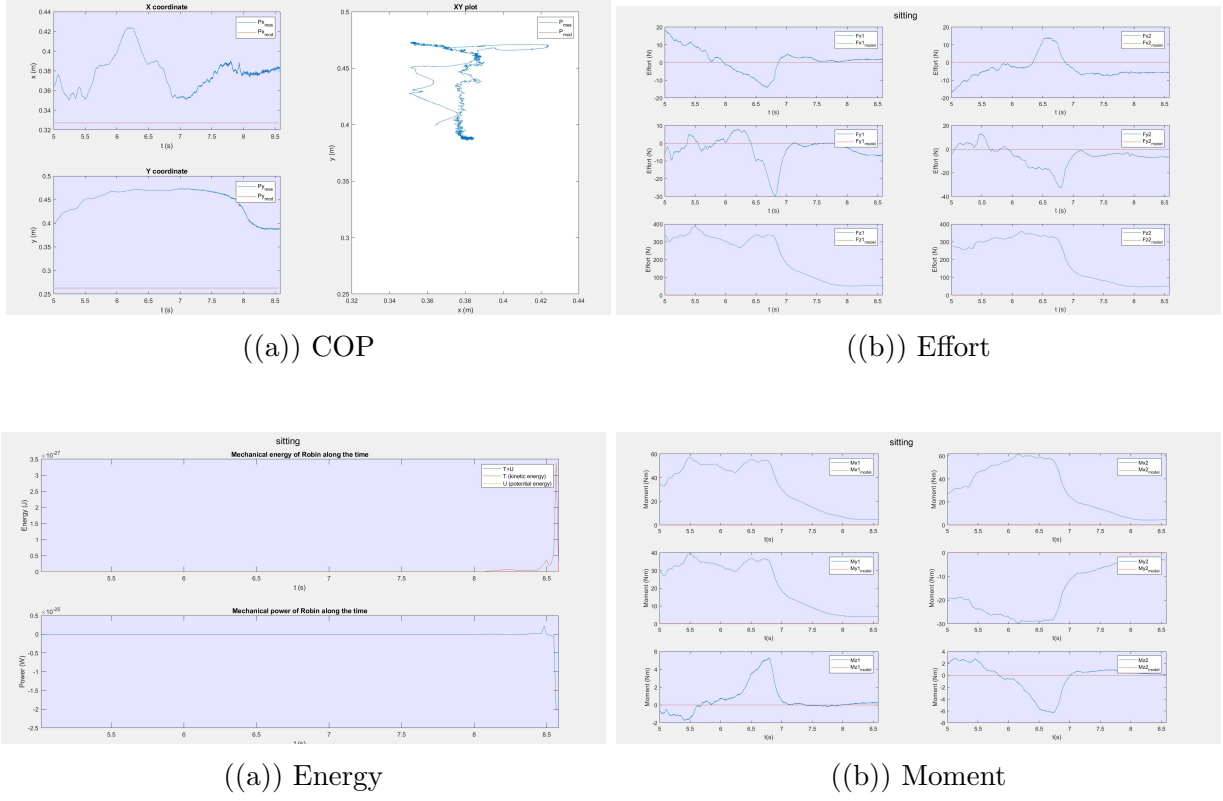


((a)) Fz

((b)) Moment Error

The above plots are representation of the High Jump motion.

5.4 Sitting Motion



The above plots are representation of the sitting on a chair motion.

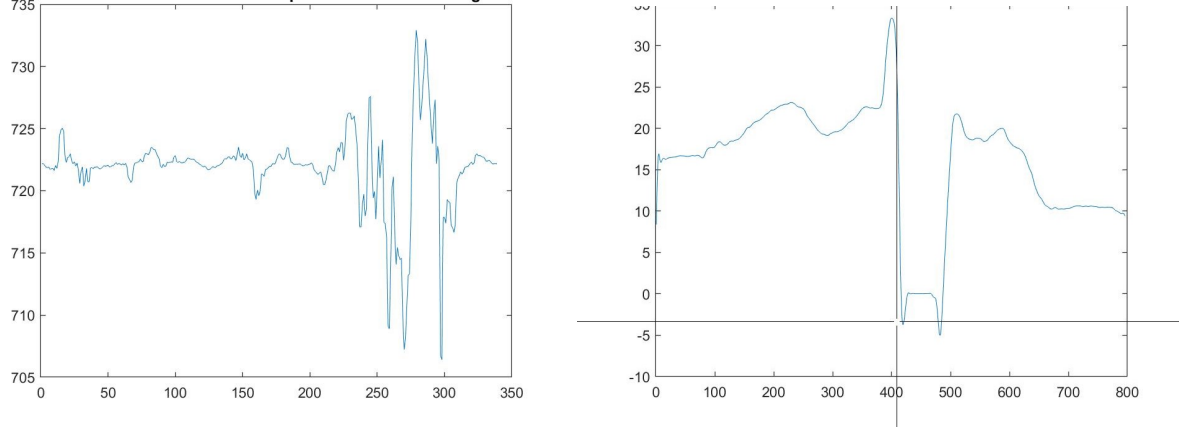
6 Synthesis

first The most difficulties we faced during the experimentation is We had to choose the correct readings from the motion capture system in order to use it for the experiment.

Then next difficulty is while capturing motions we had to look carefully to see whether the motion capture system loses track of a marker on the actor. If this happens then the data is not recorded.

Another big difficulty we faced during the experiment is We faced big difficulty when saving the captured motions in .drf format after saving when we start our next motion capture experiment we were not able to save due to the maintenance being carried out on the same intermittently affecting the software. After we must restart our process from beginning to rectify this problem. The software of the ART T rack motion caption system has a limited buffer size which means that the buffer gets filled up very quickly and caused the program to crash. We overcame this problem by only starting the capture when we require the actor to perform a motion otherwise the buffer is closed at all other times.

while comparing the reaction forces obtained by the mathematical model and the measurements obtained by the force plate We can clearly notice the same evolution of the ground reaction forces and of the forces predicted by our model up to some scaling factor.



((a)) Forces Measured from the force plate ((b)) Forces calculated from the Newton Eule

Here we extract the forces in the last segment during this motion that is in contact with the environment and compare it with the forces measured on the force plate during this same motion.

The scaling errors seen in the Newton-Euler calculated the forces is probably due to discrepancy between the model and the real human body seen the complexity of the human articulation which can hardly be geometrically modeled and Numerical derivation errors due to the truncation of the higher order derivatives during the Taylor series expansion.

We propose that this methodology can be used to closely represent the human motion as we see from the above plot that the forces are bounded and closely resemble those measured on the force plate, therefore can be reproduced on a robotics system.

7 Conclusion

The Measurement of the segments of the actor is performed and analysed. Then we implemented the Modified Hanavan model accordingly. By using motion capture system we captured the motion of the actor (Robin) and his analysis. by taking note into these motion captures we sucessfully implemented Newton-Euler equations to compute the moments ansd forces of the actor(Robin). Finally we validated the results which obtained through simulation and animation.

Acknowledgement

We sincerely thank Prof. Sophie sakka for providing us with this LAB. It has been a very enriching experience.

we would like to express our deepest gratitude for all the support,advice, instruction, guidance and patience of my supervisor Professor Sophie sakka who guided us to work on this topic.

I extend my sincere thanks to the professor for all his assistance.